International Geology Review, Vol. 37, 1995, p. 1074–1093.

Phase-Equilibrium Controls on SiO_2 Metasomatism by Aqueous Fluid in Subduction Zones: Reaction at Constant Pressure and Temperature

CRAIG E. MANNING

Department of Earth and Space Sciences, University of California, Los Angeles, California, 90024-1567

Abstract

The mineral-fluid equilibria that govern silica redistribution by aqueous fluids in subduction zones were evaluated at constant pressure and temperature in the model system MgO-SiO_2-H_2O (MSH). At <20 kbar and <1000° C, model H_2O-SiO_2 fluids liberated via devolatilization in subducting crust will be buffered at or near quartz saturation along any specified subduction P-T path, whereas fluids in equilibrium with model metaperidotites, ranging from dunite to orthopyroxenite protoliths, have silica concentrations significantly below quartz saturation. Isothermal-isobaric flow of fluid from the slab to the mantle wedge therefore drives metasomatic reactions that increase the bulk silica content of metaperidotites and decrease the silica content of the fluid. The potential for silica metasomatism increases with depth for all subduction paths and model bulk compositions. At a given depth, the capacity for silica metasomatism increases with temperature and with abundance of forsterite relative to enstatite. Water-rock ratios required to produce metasomatic mineral assemblages decrease with increasing pressure and temperature. Mineral assemblages diagnostic of silica metasomatism at shallow subduction levels require water-rock ratios of >100 moles fluid/cm^3 rock; but at depth, flow of only several moles fluid/cm^3 rock is sufficient to produce assemblages characteristic of silica metasomatism. Decreasing temperature with time in most subduction zones suggests that the potential for silica metasomatism is greatest at early stages of convergence. Subducted ultramafic rocks showing evidence of high-temperature silica metasomatism therefore may provide windows into early subduction processes. In general, temporal changes in subduction parameters favoring increasing temperatures will enhance the potential for silica metasomatism, whereas those leading to lower temperatures should be expected to decrease the capacity for silica transfer with time.

Introduction

SUBDUCTION BRINGS TOGETHER crustal and mantle lithologies along an interface defined by the subduction shear zone. This juxtaposition of rocks of different bulk composition generates the potential for strong metasomatism associated with migrating aqueous fluids. Metasomatic transfer of trace elements in subduction-zone settings has been investigated theoretically and experimentally (e.g., Navon and Stolper, 1985; Ayers and Watson, 1993; Brenan et al., 1995) because this process plays a fundamental role in modifying the sources of subduction-related magmas (e.g., Perfit et al., 1980; Gill, 1981; Arculus and Powell, 1986; Hawkesworth et al., 1993; Pearce and Peate, 1995). Bebout and Barton (1993) assessed the likely relative extents of major-element metasomatism by estimating ranges in the solubilities of H, C, O, Si, and alkalis in aqueous fluids relative to their abundance in rocks. They demonstrated that potentials for C, Si, and alkali transport were low compared to those for incompatible elements such as H, which suggests that metasomatism of major elements should be limited to comparatively small scales in subduction zones. Although local major-element metasomatism is illustrated in numerous examples of exhumed subduction-zone rocks (e.g., Heinrich, 1982; Kobayashi et al., 1987; Peacock, 1987; Sorenson, 1988; Bebout and Barton, 1989, 1993; Bebout, 1991; Früh-Green, 1994; Harlow, 1995), there are few quantitative constraints on mineral-fluid equilibria at subduction conditions, which means that critical questions about mass transfer in these localities remain unanswered. For example, how does the potential for metasomatism vary with mineral stability (i.e., P and T)? At what conditions will metasomatic mass transfer

0020-6814/95/158/1074-20 $10.00

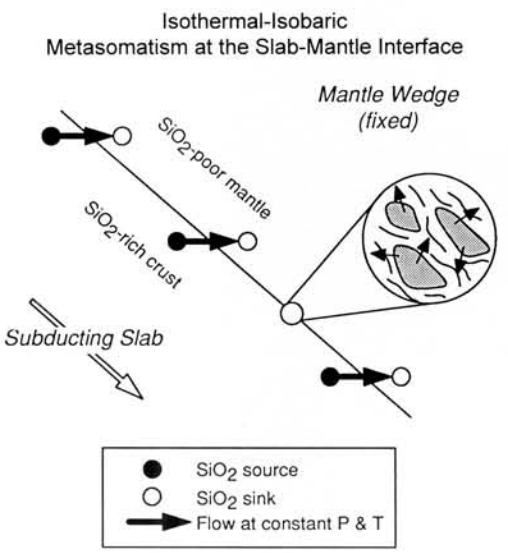

FIG. 1. Conceptual model used for analysis of flow of H_2O-SiO_2 fluid from slab to mantle wedge at constant pressure and temperature. The mantle wedge is assumed to be spatially fixed relative to the underthrusting slab. In detail, processes at the slab-mantle interface probably involve intimate interslivering of diverse lithologies. This analysis is appropriate for evaluating transfer from silica-rich blocks to a silica-poor matrix (inset), or vice versa, as long as variations in chemical-potential gradient of SiO_2 arise predominantly from lithologic contrasts rather than P and T.

be maximized? And what water-rock ratios are required to generate observed metasomatic effects? Answers to such questions require systematic exploration of metasomatic phase relations for appropriate chemical systems.

Recently completed experimental studies of the solubility of quartz in H_2O at high pressures (Manning, 1994) now allow investigation of the phase-equilibrium controls on metasomatism of a major rock-forming component (SiO_2) in subduction environments. A necessary first step toward detailed metasomatic models is an analysis of the effect of flow across lithologic contacts at constant pressure and temperature. In this paper, I examine isothermal-isobaric reactions at the slab-mantle interface along different subduction P-T paths using the simple system MgO-SiO_2-H_2O. Results in the model system provide a guide for interpretation of natural, metasomatized peridotites and yield insights into the controls on major-element metasomatism in subduction zones.

Background

Metasomatic reactions along the path of a flowing aqueous fluid are driven by changes in element solubility arising from gradients in bulk composition, P, and T. Metasomatism in subduction zones is complex, because the gradients in all three variables may be significant. To begin to unravel the phase-equilibrium controls on SiO_2 redistribution, an appropriate starting point is the assessment of isothermal-isobaric reactions driven only by lithologic variation along the flow path. This is the focus of the present paper. The analysis provides the background for more complex models of flow and reaction on paths along which P, T, and bulk composition vary (Manning, 1996a).

The reference frame for evaluating silica metasomatism at constant P and T is illustrated in Figure 1. The mantle wedge is assumed to be stationary (see below), and the subducting slab moves beneath it along the subduction shear zone. The sources of aqueous fluid are the silica-rich crustal lithologies of the subducting slab. That fraction of fluid that flows across the subduction shear zone migrates into the silica-poor mantle wedge at constant P and T. In detail, the lithologic contrasts in the vicinity of the subduction shear zone may be structurally complex, probably consisting of a melange of different lithologies (e.g., Bebout and Barton, 1989, 1993), but these features simply reflect small-scale examples of the same lithologic variations implied by flow across an infinitesimally narrow shear-zone contact between crustal and mantle lithologies (Fig. 1). Thus, regardless of the actual geometry of lithologic contacts, an analysis of isothermal-isobaric mass transfer is relevant to metasomatism at scales of a few tens of meters or less, where chemical-potential differences caused by changes in P and T probably are small compared to those arising from bulk-compositional contrasts.

In addition to P, T, and bulk composition, the extent of metasomatism also is controlled by the kinetics of reaction, the geometry of the pore network, and the volume of fluid. To investigate phase-equilibrium controls on metasomatic reactions, equilibrium is assumed and fluid migration is taken to be by porous flow, such that complete exchange between fluid and rock occurs. Thus, if the volume of isothermal-isobaric fluid flow is specified,

metasomatic variations will result from (1) the gradient in the chemical potential of SiO_2, as determined by the starting fluid composition and the bulk composition of the mantle wedge, and (2) the P-T path of subduction, which dictates the conditions at which reaction occurs.

Starting fluid composition

This study assumes a model, two-component H_2O-SiO_2 fluid. A complete analysis would require consideration of CO_2, NaCl, and other components, but the effect of fluid composition on SiO_2 solubility has not been investigated experimentally or theoretically at the high pressures of subduction zones. Moreover, a two-component fluid is useful because SiO_2 concentrations in aqueous fluids typically are significantly greater than other components at moderate to high pressures (e.g., Eugster and Baumgartner, 1987; Manning and Boettcher, 1994), so the simplified composition provides a first-order understanding of the phase-equilibrium controls on SiO_2 metasomatism.

At a given P and T, the starting SiO_2 content of aqueous fluids in the slab will be controlled by the minerals present when dehydration reactions occur. The volumetrically dominant slab lithology near the subduction shear zone will be mafic in composition. Studies of metabasalts along high-P/T facies series show that quartz typically is present until anhydrous, eclogite-facies mineral assemblages develop (e.g., Ernst, 1990; Peacock, 1993a). Fluids liberated from hydrous metabasalts therefore will be quartz saturated. Moreover, downgoing slabs are probably mantled by a veneer of sediment that is dominated by pelagic material (Moore, 1975; Plank and Langmuir, 1993). The compositions of ocean-floor sediments are sufficiently silica-rich (Hay et al., 1988; Kyte et al., 1993; Plank, 1993) that their metamorphic equivalents will contain substantial modal volumes of quartz (e.g., Ernst, 1990), and quartz saturation is likely to persist as fluid is lost during subduction (Manning, 1996b). In addition, oceanic mantle lithosphere also may be a significant source of fluids in the downgoing slab (e.g., Thompson, 1992; Scambelluri et al., 1995; Ulmer and Trommsdorff, 1995); however, unless in direct contact with mantle-wedge lithologies, fluids produced in hydrous mantle rocks can be expected to flow through and equilibrate with quartz-bearing metabasalt or metasediment. Thus, fluids produced in the slab are assumed here to be quartz saturated prior to flow into the mantle wedge.

Subduction P-T paths

As illustrated in Figure 1, the mantle wedge is postulated as stationary; that is, it does not deform during metasomatic reaction. Although the dynamics of mantle deformation in subduction zones are poorly understood, the region along the slab-mantle interface where this assumption is most likely to hold is the mechanical lithosphere (e.g., Davies and Stevenson, 1992; Peacock, 1993b), which is here assumed to correspond to conditions at which $P<20$ kbar and $T<1000°$ C. Because these are the conditions at which much (but not all) of the fluid production occurs in the slab (Peacock, 1990, 1993a), it is an appropriate subdivision of P-T space for analysis of the phase-equilibrium controls on metasomatic mass transfer.

Figure 2A shows three P-T paths corresponding to the slab-mantle interface to a vertical depth of ~70 km, or ~200 km of slab length. The P-T paths are those of Peacock (1993a), in which the steady-state thermal regimes were calculated for subduction at 10 cm/yr, a subduction angle of 20°, rock densities of 3.0 g/cm^3, and increasing shear stress from Path 3 (33 MPa) through Path 2 (67 MPa) to Path 1 (100 MPa). Because the subduction paths differ in their temperatures at a given depth, they can be used to illustrate a range in P-T conditions resulting from different subduction scenarios. For example, Path 1 represents the P-T regime that might be expected when young oceanic crust is subducted, whereas Path 3 probably best reflects conditions likely in a long-lived subduction zone and represents an approximate lower limit on likely subduction-zone temperatures (Peacock, 1993a). Although different, more complex P-T paths may result from consideration of the brittle–ductile transition (Peacock et al., 1994) or alternative numerical analyses of heat and mass transfer (e.g., Davies and Stevenson, 1992), the paths used here serve to illustrate the effects of different P-T paths on SiO_2 metasomatism at the slab-mantle interface. Note that the steady-state conditions of this analysis dictate that heat liberated or consumed by reaction does not affect the thermal

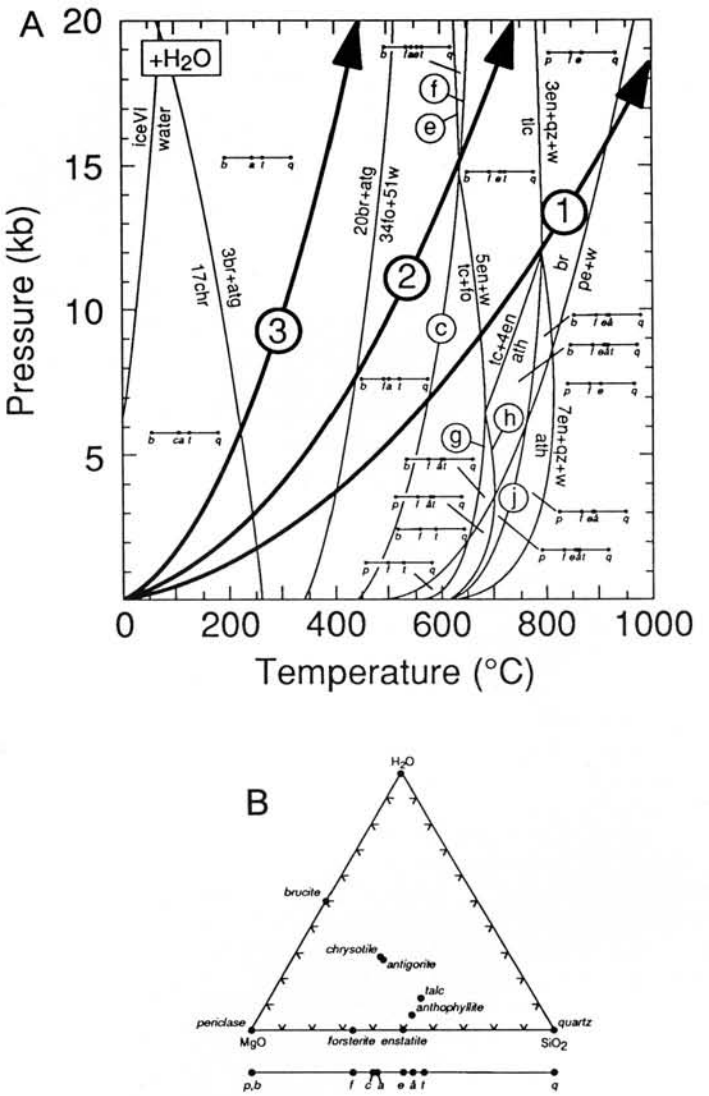

FIG. 2. A. Stable phase equilibria in the system MgO-SiO_2-H_2O in the presence of excess H_2O calculated using the GEO-CALC computer program (Berman et al., 1987). Equilibria are listed in Table 1. Quartz and enstatite are in their stable structural states at all P and T, although the transition boundaries were omitted for clarity. The water–ice phase boundary is from Haselton et al. (1995). P-T paths (bold arrows) are from Peacock (1993a). B. MgO-SiO_2-H_2O ternary and H_2O-excess binary showing phase compositions (a° = anthophyllite).

regime, which is reasonable for most subduction scenarios (Davies and Stevenson, 1992).

Model composition of the mantle wedge

Phase relations were evaluated in the system MgO-SiO_2-H_2O (MSH) to approximate the bulk composition of mantle lithosphere present above subducting slabs. Potentially important components not considered are FeO, Al_2O_3, and CaO. The advantage of ignoring these components is that analysis of phase relations in the simple MSH system allows evaluation of the controls on metasomatism, which then provides a framework for more complex analyses involving the additional phases required by other components. It is particularly important to rec-

ognize, however, that addition of small amounts of FeO leads to large shifts in the positions of equilibria in Figure 2A (e.g., Evans and Guggenheim, 1988), leading most importantly to increased stability of Ca-free amphibole. Ca-free amphibole (anthophyllite or cummingtonite) therefore should be more common in natural, Fe-bearing peridotites than its stability field in Figure 2A would suggest. However, shifts in the locations of individual equilibria and invariant points from addition of FeO do not change the fundamental metasomatic topologies relative to those of the simple MSH system.

Bulk compositions ranging from forsterite to enstatite were examined to investigate the effect of a range in Mg/Si ratios on metasomatic phase relations. The minerals considered are shown in Figure 2B in the ternary MgO-SiO_2-H_2O, and projected to the excess-H_2O binary join between MgO and SiO_2. Lizardite is not included in the calculations because the thermodynamic properties of Fe-Al-free end member are poorly known. In addition, although field evidence suggests lizardite is a stable serpentine polymorph (e.g., Wicks and O'Hanley, 1988), all experimental syntheses appear to be metastable with respect to antigorite and chrysotile, which implies that Al-free lizardite can be stable only at low temperatures (e.g., $<250°$ C at 2 kbar) (Chernosky et al., 1988), if at all. Thus, natural occurrences of lizardite likely reflect low temperatures or stabilization by minor Al or Fe^{3+} substitution into the crystal structure. Because of the higher temperatures and Al- and Fe-free bulk composition considered here, lizardite need not be considered further. Other low-temperature minerals not considered here are sepiolite, hypothetical MSH palygorskite, and the Mg-montmorillonite stevensite, which all are metastable with respect to talc and chrysotile (Hostetler and Christ, 1968; Jones, 1986; Stoessel, 1988; Jones and Gallan, 1988).

High-temperature, high-pressure phases excluded from this study include the humite-group minerals, phases "A" through "F," and 10-Å $Mg_3Si_4O_{10}(OH)_2 \cdot 2H_2O$ (Sclar and Carrison, 1966; Ringwood and Major, 1967; Yamamoto and Akimoto, 1974, 1977; Bauer and Sclar, 1979, 1981; Akimoto and Akiogi, 1980; Liu, 1986, 1987; Kanzaki, 1991; Thompson, 1992; Luth, 1995; Bose and Ganguly, 1995; Pawley et al., 1995; Pawley and Wood, 1995). Their thermodynamic properties are poorly known, but analyses of phase relations by Yamamoto and Akimoto (1977), Liu (1987), Bose and Ganguly (1995), and Pawley and Wood (1995) show that these minerals are not likely to be stable at $\leq$20 kbar for bulk compositions between forsterite and enstatite. Partial melting of MSH bulk compositions between forsterite and enstatite does not occur under the P-T conditions evaluated (Kushiro et al., 1968b; Ellis and Wyllie, 1979; Ito and Weidner, 1986; Kanzaki, 1991), although the water-saturated solidi of natural peridotites are intersected at $<1000°$ C at $\sim$10 to 20 kbar (Kushiro et al., 1968a; Kushiro, 1970; Green, 1973; Millhollen et al., 1974; Mysen and Boettcher, 1975).

Thermodynamic calculations employed equations and data of Haar et al. (1984) for H_2O, Berman (1988) for minerals, and Manning (1994) for aqueous silica. Minerals were assumed to be stoichiometric and to have unit activity at all values of P and T. Despite experimental difficulties in determining chrysotile stability, Berman et al. (1986) and Berman (1988) assumed it to be a stable phase at low temperatures based on its widespread occurrence in natural serpentinites. Mineral compressibilities of Berman (1988) were assumed to hold over the pressure range investigated (up to 20 kbar), although recent analyses of talc (Bose and Ganguly, 1995; Pawley et al., 1995) suggest that extrapolation to higher pressures would be inaccurate. The thermodynamic properties of the fluid were approximated by pure H_2O because of the low mole fractions of dissolved SiO_2 over the P-T range of the study.

Figure 2A and Table 1 provide stable phase equilibria relevant to high-pressure metamorphism in the MSH system in the presence of excess H_2O. Figure 2A is similar to P-T projections provided by Berman et al. (1986) and Evans and Guggenheim (1988), with the exception that equilibria were projected from H_2O. Phase boundaries are consistent with the recent studies of Johnson and Walker (1993), Pawley and Wood (1995), Bose and Ganguly (1995), and Ulmer and Trommsdorff (1995). The P-T projection is consistent with the results of Chernosky et al. (1985), but differs from the

TABLE 1. Selected Equilibria in the System $MgO\text{-}SiO_2\text{-}H_2O$[1]

a. $17Mg_3Si_2O_5(OH)_4 = 3Mg(OH)_2 + Mg_{48}Si_{34}O_{85}(OH)_{62}$
chrysotile brucite antigorite

b. $20Mg(OH)_2 + Mg_{48}Si_{34}O_{85}(OH)_{62} = 34Mg_2SiO_4 + 51H_2O$
brucite antigorite forsterite

c. $Mg_{48}Si_{34}O_{85}(OH)_{62} = 4Mg_3Si_4O_{10}(OH)_2 + 18Mg_2SiO_4 + 27H_2O$
antigorite talc forsterite

d. $Mg_3Si_4O_{10}(OH)_2 + Mg_2SiO_4 = 5MgSiO_3 + H_2O$
talc forsterite enstatite

e. $Mg_{48}Si_{34}O_{85}(OH)_{62} + 14Mg_3Si_4O_{10}(OH)_2 = 90MgSiO_3 + 45H_2O$
antigorite talc enstatite

f. $Mg_{48}Si_{34}O_{85}(OH)_{62} = 14Mg_2SiO_4 + 20MgSiO_3 + 31H_2O$
antigorite forsterite enstatite

g. $9Mg_3Si_4O_{10}(OH)_2 + 4Mg_2SiO_4 = 5Mg_7Si_8O_{22}(OH)_2 + 4H_2O$
talc forsterite anthophyllite

h. $Mg_7Si_8O_{22}(OH)_2 + Mg_2SiO_4 = 9MgSiO_3 + H_2O$
anthophyllite forsterite enstatite

i. $Mg_7Si_8O_{22}(OH)_2 = Mg_3Si_4O_{10}(OH)_2 + 4MgSiO_3$
anthophyllite talc enstatite

j. $7Mg_3Si_4O_{10}(OH)_2 = 3Mg_7Si_8O_{22}(OH)_2 + 4SiO_2 + 4H_2O$
talc anthophyllite quartz

k. $Mg_7Si_8O_{22}(OH)_2 = 7MgSiO_3 + SiO_2 + H_2O$
anthophyllite enstatite quartz

l. $Mg_3Si_4O_{10}(OH)_2 = 3MgSiO_3 + SiO_2 + H_2O$
talc enstatite quartz

m. $Mg(OH)_2 = MgO + H_2O$
brucite periclase

[1]Reactant assemblage stable at low temperature and fixed pressure.

projections of Delany and Helgeson (1978), which assume that antigorite is not stable with chrysotile (Helgeson et al., 1978).

Path 1 traverses Figure 2A at the highest temperatures at any given pressure. This low P-T path passes slightly above the maximum stability of anthophyllite, which makes this phase metastable at all conditions evaluated in the present study. Because of the positive Clapeyron slope of the reaction brucite + antigorite = forsterite + water, forsterite is produced at the lowest temperature and shallowest depths along Path 1. Moreover, all initial bulk compositions (Mg/Si = 2 to 1) will contain forsterite and enstatite in the presence of H_2O at the shallowest levels on this path. Path 2 represents intermediate P-T conditions. Because it passes above the enstatite-antigorite-forsterite-talc-H_2O invariant point, this path will produce the unusual assemblage enstatite + antigorite for appropriate bulk compositions (see below). The anhydrous assemblage forsterite + enstatite is stable with H_2O at somewhat lower temperature than along Path 1, but at significantly greater depth. Path 3 represents high P-T subduction paths. The only univariant equilibrium crossed below 20 kbar is the H_2O-conserving transformation of chrysotile to antigorite + brucite.

Because $SiO_{2(aq)}$ mole fractions are low in the P-T range considered (see below), and because full hydration of model MSH peridotites requires comparatively little H_2O (Bebout and Barton, 1993), the starting mineral assemblages in the mantle wedge can be assumed to be those in equilibrium with H_2O everywhere along the

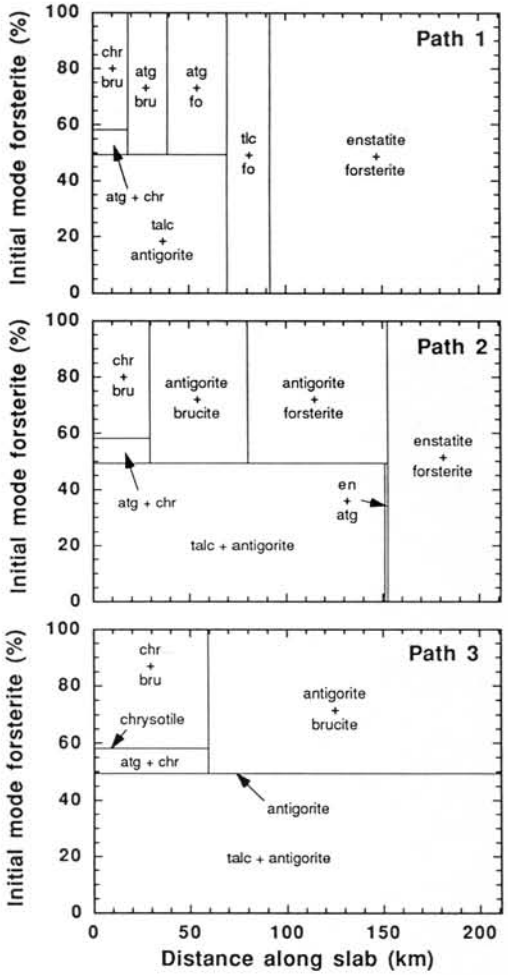

FIG. 3. Fully hydrated model MSH peridotite assemblages as a function of distance along the slab and initial forsterite mode for Paths 1, 2, and 3.

subduction path. This is tantamount to assuming that prior to SiO_2 metasomatism, sufficient quantities of pure H_2O react fully with the mantle wedge so that it is everywhere H_2O saturated. Figure 3 shows the starting H_2O-saturated mantle-wedge mineral assemblages as a function of the initial ratio of forsterite to enstatite (V^{o}_{fo}) and distance along the subduction zone as calculated using the reaction coefficients given in Table 2 (cf. Kitahara et al., 1966; Yamamoto and Akimoto, 1977; Liu, 1987). Fields in these diagrams correspond to divariant assemblages, horizontal lines to trivariant assemblages, and vertical lines to univariant MSH equilibria (Fig. 2A). The convergence of all paths at low P and T results in identical, low-grade mineral assemblages in the presence of H_2O: chrysotile + brucite where $Mg/Si > 3/2$, antigorite + chrysotile where $3/2 > Mg/Si > 48/34$, and talc + antigorite where $Mg/Si < 48/34$. P and T increase along each path, but to differing degrees. Along Path 3 (Fig. 3C), low temperatures persist to high pressures. This results in little change in the hydrous MSH assemblage along the entire path because only one reaction boundary is crossed. Thus Path 3 generates comparatively large regions of stability of individual assemblages in distance–bulk composition space. The higher temperatures of Path 2 mean that more univariant equilibria are intersected (Fig. 2A), and the stability regions of low-T assemblages diminish at the expense of high-temperature assemblages such as antigorite + forsterite, enstatite + antigorite, and enstatite + forsterite (Fig. 3B). Path 1 results in the highest temperatures at a given distance, producing hydrous-phase stabilities that are spatially and compositionally the most restricted. For enstatite-rich bulk compositions, the assemblage talc + antigorite is stable along much of the slab-mantle interface, whereas mineral assemblages are more variable for forsterite-rich bulk compositions.

Silica Metasomatism along the Slab-Mantle Interface

Quartz solubility and subduction P-T paths

Measured quartz solubilities at high pressures and temperatures allow prediction of the concentration of SiO_2 in H_2O equilibrium with quartz from 25° C, 1 bar to >20 kbar and ~1000° C (Manning, 1994). Values of the logarithm of aqueous silica molality ($\log m_{SiO_2(aq)}$) at quartz-H_2O equilibrium are shown as a function of P and T in Figure 4, where it can be seen that quartz solubility increases strongly with increasing pressure and temperature. Along Paths 1, 2, and 3, quartz solubility increases from $\sim 10^{-4}$ molal at 25° C, 1 bar (6.0 ppm), to respectively 0.2 molal (0.9 wt%), 1.5 molal (8.1 wt%), and 5.2 molal (24.0 wt%) at the highest temperature.

The increases in silica solubility at quartz saturation of 10^3 to $10^{4.5}$ times along the P-T

TABLE 2. Reaction Coefficients of H_2O and Secondary Minerals for Hydration of Model Peridotites[1]

Stable secondary assemblage	H_2O	Brucite	Chrysotile	Antigorite	Talc	Forsterite	Enstatite
Brucite + chrysotile	$\frac{3n_f^o + n_e^o}{2}$	$\frac{n_f^o - n_e^o}{2}$	$\frac{n_f^o + n_e^o}{2}$				
Chrysotile + antigorite	$\frac{3n_f^o + n_e^o}{2}$		$\frac{10n_f^o - 7n_e^o}{3}$	$\frac{n_e^o - n_f^o}{6}$			
Antigorite + talc	$\frac{3n_f^o + n_e^o}{2}$			$\frac{5n_f^o + n_e^o}{90}$	$\frac{7n_e^o - 10n_f^o}{45}$		
Antigorite + brucite	$\frac{51n_f^o + 17n_e^o}{34}$	$\frac{10n_f^o - 7n_e^o}{17}$		$\frac{n_f^o + n_e^o}{34}$			
Forsterite + antigorite	$\frac{31n_e^o}{20}$			$\frac{n_e^o}{20}$		$n_f^o - \frac{14n_e^o}{20}$	
Forsterite + talc	$\frac{n_e^o}{5}$				$\frac{n_e^o}{5}$	$n_f^o + \frac{n_e^o}{5}$	
Enstatite + antigorite	$\frac{31n_f^o}{14}$			$\frac{n_f^o}{14}$			$n_e^o - \frac{20n_f^o}{14}$
Forsterite + enstatite						n_f^o	n_e^o

[1] n_f^o = initial forsterite content (moles); n_e^o = initial enstatite content (moles). Coefficients were derived using molar volumes from Berman (1988) by simultaneously solving Mg, Si, and H mass-balance expressions for each assemblage.

paths demonstrate that subduction generates large gradients in fluid transport capacities that depend on P and T (see also Bebout and Barton, 1993; Manning, in press, 1996a, 1996b); but analysis of isothermal-isobaric metasomatism requires simultaneous consideration of the effect of bulk composition at each P and T along the subduction path (e.g., Thompson, 1959; Khorzhinskii, 1964, 1965; Helgeson, 1967, 1970; Hemley et al., 1977a, 1977b). This is particularly important in the case of silica metasomatism in subduction zones because of the large gradients in the chemical potential of SiO_2 between the Si-rich slab and the Si-poor mantle wedge. The combined effects of P, T, and bulk composition on metasomatic phase relations can be assessed through phase diagrams illustrating the dependence of fluid composition on mineral stability.

Metasomatic phase diagrams

Equilibria among $SiO_{2(aq)}$ and minerals in the MSH system were computed along each subduction path using the thermodynamic data for aqueous silica calculated as described by Manning (1996a, 1996b) and the equilibria presented in Table 3. By adopting standard states of unit activity of pure phases at any temperature and pressure and unit activity of a one-molal solution at infinite dilution and any pressure and temperature, and by equating $SiO_{2(aq)}$ activity to its molality (e.g., Hemley et al., 1977b; Walther and Helgeson, 1977; Walther and Orville, 1983), the mass-action expressions for the reactions in Table 3 describe the dependence of mineral stability on $SiO_{2(aq)}$ concentration and position along subduction paths. Reactions in Table 3 employ the conventional silica species $SiO_{2(aq)}$. This avoids uncertainties about silica hydration state by assuming that the thermodynamic properties of hydrated silica are the sum of those of $SiO_{2(aq)}$ and H_2O. Thus, explicit provision for hydration of aqueous silica would change the stoichiometries of H_2O in the equilibria in Table 3 (e.g., Hemley et al., 1977b), but would not alter the thermo-

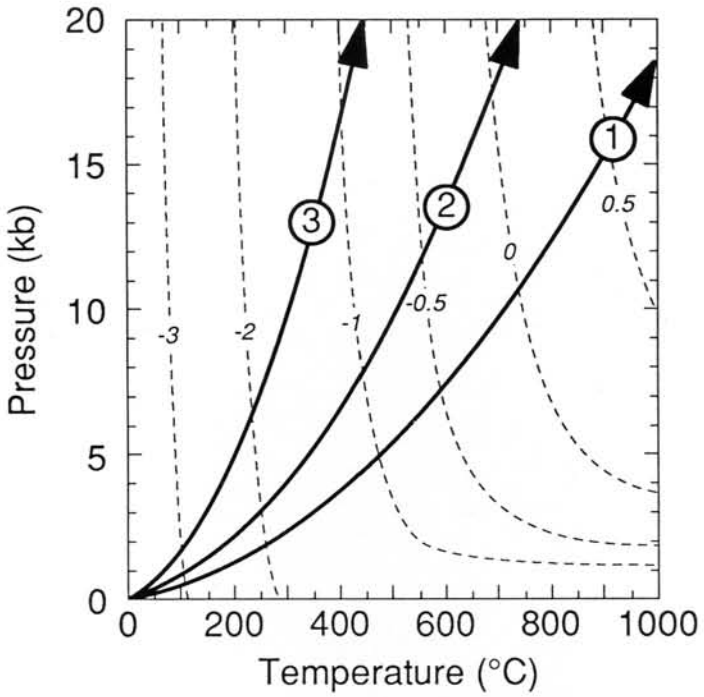

FIG. 4. Concentration of aqueous silica (log molality) in equilibrium with quartz from the results of Manning (1994).

dynamic properties of the reactions (Walther and Helgeson, 1977; Walther and Orville, 1983).

Figure 5 shows phase relations along each subduction path as a function of $\log m_{SiO_{2(aq)}}$. The diagrams are similar to isobaric diagrams of Hemley et al (1977a, 1977b) and Evans and Guggenheim (1988), except that P and T covary along the ordinates. Along a specified subduction path, mineral pairs are univariant in the presence of a fluid: they fix $m_{SiO_{2(aq)}}$ at a given point along the slab-mantle interface and they buffer $m_{SiO_{2(aq)}}$ as P and T change. The widths of divariant one-phase fields define the range in Si concentration over which the phase is stable. These fields therefore indicate regions in which both $m_{SiO_{2(aq)}}$ and position in the subduction zone may vary independently. Invariant points are defined by the coexistence of three minerals with an H_2O-SiO_2 fluid. They fix both solution composition and position along the path.

In Figure 5, the maximum equilibrium concentration of $SiO_{2(aq)}$ is defined by quartz saturation along each path. Silica concentrations in excess of quartz saturation do not reflect equilibrium; such fluids equilibrate by precipitating quartz, thereby decreasing their $SiO_{2(aq)}$ content. Fluids with $SiO_{2(aq)}$ contents lower than quartz saturation at any P and T reflect equilibrium with quartz-undersaturated bulk compositions. Isothermal, isobaric phase relations involving an Si-bearing pore fluid (Fig. 5) may be considered for two hypothetical cases (cf. Hemley et al., 1977b)—reactions in a closed system with static pore fluid, and reactions in an open system involving a flowing pore fluid.

Phase relations in closed systems

In fully hydrated MSH peridotites that are closed with respect to mass exchange with the adjacent slab, the $SiO_{2(aq)}$ concentration in the pore fluid is controlled by rock bulk composition. Figure 5 shows that Si-exchange equilibria between all mineral pairs (Table 3) have positive slopes, which means that $SiO_{2(aq)}$ concentration in mantle-wedge pore fluids near the slab increases with depth in the subduction zone,

TABLE 3. Relevant Silicification Equilibria in the System $MgO\text{-}SiO_2\text{-}H_2O$[1]

a. $3Mg(OH)_2 + 2SiO_{2(aq)} = Mg_3Si_2O_5(OH)_4 + H_2O$
brucite — chrysotile

b. $48Mg(OH)_2 + 34SiO_{2(aq)} = Mg_{48}Si_{34}O_{85}(OH)_{62} + 17H_2O$
brucite — antigorite

c. $16Mg_3Si_2O_5(OH)_4 + 2SiO_{2(aq)} = Mg_{48}Si_{34}O_{85}(OH)_{62} + H_2O$
chrysotile — antigorite

d. $Mg_{48}Si_{34}O_{85}(OH)_{62} + 30SiO_{2(aq)} = 16Mg_3Si_4O_{10}(OH)_2 + 15H_2O$
antigorite — talc

e. $3MgSiO_3 + SiO_{2(aq)} + H_2O = Mg_3Si_4O_{10}(OH)_2$
enstatite — talc

f. $Mg_2SiO_4 + SiO_{2(aq)} = 2MgSiO_3$
forsterite — enstatite

g. $3Mg_2SiO_4 + 5SiO_{2(aq)} + 2H_2O = 2Mg_3Si_4O_{10}(OH)_2$
forsterite — talc

h. $24Mg_2SiO_4 + 10SiO_{2(aq)} + 31H_2O = Mg_{48}Si_{34}O_{85}(OH)_{62}$
forsterite — antigorite

i. $Mg_{48}Si_{34}O_{85}(OH)_{62} + 14SiO_{2(aq)} = 48MgSiO_3 + 31H_2O$
antigorite — enstatite

j. $2MgO + SiO_{2(aq)} = Mg_2SiO_4$
periclase — forsterite

k. $2Mg(OH)_2 + SiO_{2(aq)} = Mg_2SiO_4 + H_2O$
brucite — forsterite

[1]Reactant assemblage stable at low $SiO_{2(aq)}$ activity at fixed temperature and pressure.

regardless of bulk composition. For example, for $V^o_{fo} = 80\%$, the mineral assemblage stable at low pressures and temperatures is chrysotile + brucite (Fig. 3), so $SiO_{2(aq)}$ concentration will be buffered by this phase boundary below 10^{-6} molal at shallow levels of subduction zones, regardless of P-T path. As depth increases, $m_{SiO_2(aq)}$ becomes greater until the chrysotile-brucite-antigorite invariant point is reached at $m_{SiO_2(aq)} \sim 10^{-5}$ and the mineral assemblage converts to antigorite + brucite. Depending on P/T, the new antigorite + brucite assemblage may continue to buffer $m_{SiO_2(aq)}$ to beyond 20 kbar (Path 3), or additional invariant points may be encountered (Paths 1 and 2). For example, along Path 2, $SiO_{2(aq)}$ concentration increases with depth as controlled by brucite + antigorite stability until the brucite + antigorite + forsterite invariant point is encountered at ~8 kbar and $\log m_{SiO_2(aq)} = -3.2$, and the mineral assemblage converts to forsterite + antigorite. At greater depths, the concentration of $SiO_{2(aq)}$ continues to increase to the next invariant point, where forsterite + enstatite become stable. Note that talc does not appear for this bulk composition because of the narrow stability field of antigorite + enstatite (Figs. 2A and 5). In general, the changes in the composition of stationary pore fluid in an isochemical, stationary rock volume in the mantle wedge can be determined by identifying the progression of mineral assemblages for a given bulk composition in Figure 3, and then determining the $SiO_{2(aq)}$ concentration required for the position on the path of interest in Figure 5.

Figure 5 shows that the $SiO_{2(aq)}$ content of static pore fluids in model MSH peridotites increase with increasing depth in subduction zones, regardless of P-T path or starting model bulk composition. All three paths begin at 1 bar and 1° C, where chrysotile + brucite in fully hydrated forsterite-rich bulk compositions ($Mg/Si > 3/2$) buffer $SiO_{2(aq)}$ concentration at $10^{-9.75}$ molal. More enstatite-rich compositions

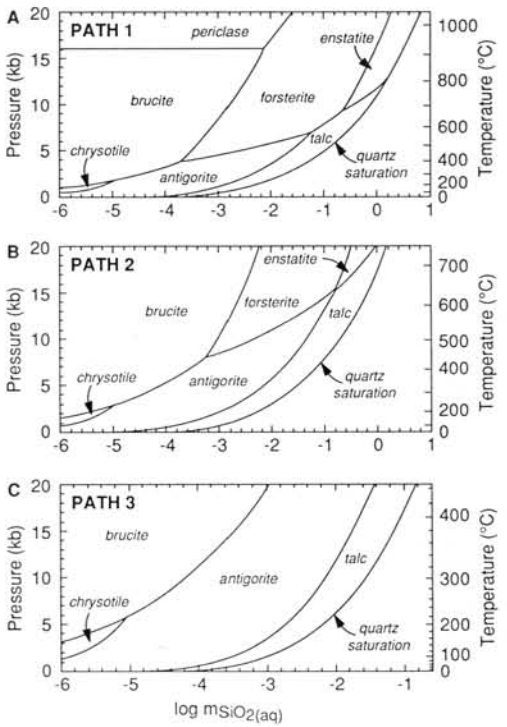

FIG. 5. Metasomatic phase diagrams showing mineral-solution equilibria along Paths 1-3 in the system MgO-SiO_2-H_2O. P and T covary along the ordinates.

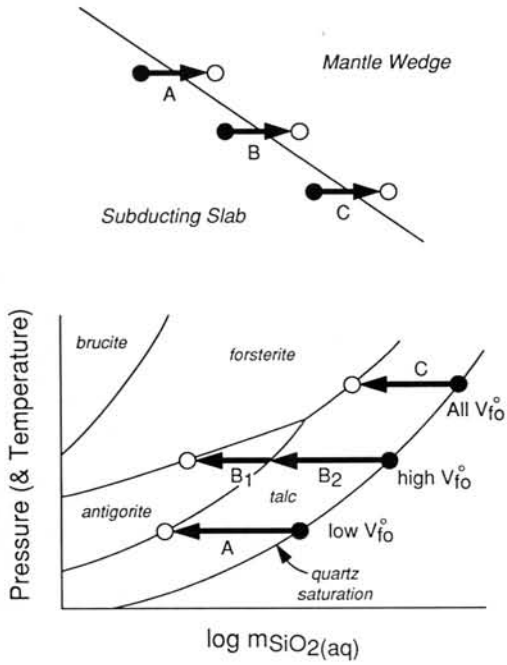

FIG. 6. Schematic diagram showing framework for evaluating isothermal-isobaric metasomatic reactions along the slab-mantle interface at different depths and initial fosterite-enstatite ratios.

lead to $10^{-7.72}$ (antigorite + brucite, $3/2 > Mg/Si > 48/34$) and $10^{-4.94}$ molal (antigorite + talc, $48/34 > Mg/Si > 1$). At 20 kbar along Path 3, antigorite + brucite equilibrium requires $SiO_{2(aq)} = 10^{-2.84}$ molal, so $m_{SiO_2(aq)}$ in a static wedge pore fluid increases by nearly seven orders of magnitude. More enstatite-rich bulk compositions are composed of antigorite + talc to 20 kbar, where $m_{SiO_2(aq)} = 10^{-1.37}$. The increase in $SiO_{2(aq)}$ molality for these more silica-rich bulk compositions is thus ~3.5 orders of magnitude to 20 kbar. Along the higher temperature paths, forsterite + enstatite are stable at 20 kbar, so pore-fluid composition depends only on subduction path. At 20 kbar, forsterite + enstatite require that $SiO_{2(aq)} = 10^{-0.46}$ molal on Path 2 and $10^{0.16}$ molal on Path 1. Thus, static pore fluids in the mantle wedge display increases in $m_{SiO_2(aq)}$ of about 8.5 to 9 orders of magnitude along high-temperature paths. Such large increases dramatically exceed those experienced by quartz-saturated rocks (Fig. 4).

Phase relations in open systems

Isothermal-isobaric flow of SiO_2-H_2O fluids from the silica-rich slab to the silica-poor mantle wedge will result in silica metasomatism. The metasomatic reference frame adopted here (Fig. 3) leads to reaction paths such as those illustrated in Figure 6. Flow at constant P and T requires changes in the SiO_2 content of both fluid and rock. These can be determined from Figure 5. Qualitatively, fluid in equilibrium with quartz and liberated from the slab and flowing across the subduction shear zone into a lithology with high Mg/Si decreases its $m_{SiO_2(aq)}$ at constant P and T by dissolution of the silica-poor phase and growth of the silica-rich phase (Fig. 6). Along reaction path B_1 in Figure 6, these phases correspond to forsterite and antigorite, respectively (reaction h, Table 3). Dissolution of forsterite continues until it is completely expended and a rock composed of 100% antigorite is produced. Equilibration of the next aliquot of quartz-saturated fluid requires consumption of $SiO_{2(aq)}$, which can occur only by dissolution of antigorite and

nucleation and growth of talc (reaction d, Table 3). Once this occurs, the final fluid composition shifts to antigorite-talc equilibrium, the reaction path corresponds to B_2, and antigorite dissolves as talc grows until a rock composed of pure talc is produced. The next aliquot of fluid will cause quartz to nucleate, after which there is no further net transfer of silica between rock and fluid. As illustrated by reaction paths A and C in Figure 6, the nature of the mineral-fluid reactions and the magnitudes of the required shifts in fluid composition vary depending on position in the subduction zone and initial bulk composition.

The phase-equilibrium controls on silica metasomatism resulting from flow across the slab-mantle interface were derived using the phase relations in Figure 5 and mass-balance constraints (Ferry, 1986) for a given number of moles of fluid (n_F) per cm^3 of rock. Figure 7 illustrates effects of flow of different quantities of quartz-saturated fluid on model hydrated peridotites in terms of position along the slab-mantle interface and starting bulk composition. As in Figure 3, initial bulk composition is expressed by the initial mode of forsterite to provide a convenient reference frame. At water-rock ratios only slightly greater than those causing complete peridotite hydration, phase relations in Figure 7 are similar to those in Figure 3. However, increasing water-rock ratios lead to metasomatic modification of the mineral assemblages. As n_F increases for each subduction path, the stability fields of silica-rich assemblages expand at the expense of silica-poor initial assemblages. Silica-rich assemblages expand upward from siliceous (enstatite-rich) compositions to magnesian (forsterite-rich) compositions in the diagrams. This is because less fluid is required to drive silicification reactions to completion in lithologies already rich in SiO_2. Given an increasing water-rock ratio, three-mineral zones (invariant assemblages), denoted by vertical lines in Figure 7, retreat to progressively more magnesian compositions (and eventually off the diagrams) as they are replaced by higher-variance assemblages. This pattern of increasing variance of phase assemblages is a hallmark of the metasomatic process (e.g., Thompson, 1959).

Expansion of the stabilities of silica-rich assemblages is expressed in the steepening of the slopes of monomineralic chrysotile and antigorite zones (Fig. 7). Slopes of these zones are horizontal (depth-independent) prior to SiO_2 metasomatism. After reaction with n_F moles of quartz-saturated fluid, their slopes increase with increasing depth because of the progressively greater difference between the SiO_2 content of quartz-saturated fluid and that of fluid in equilibrium with the relevant mineral assemblage. This steepening causes monomineralic mineral zones to become increasingly restricted spatially as water-rock ratios increase. Note that diffusive or advective mass transfer with updip or downdip lithologies is not considered, so the monomineralic zones have infinitesimal width. In reality, exchange with adjacent lithologies would cause monomineralic zones to widen with time (Thompson, 1959), and the extent of widening would depend on the variation in transport parameters with subduction depth.

An exception to the general pattern of steepening of monomineralic zones in modal volume-distance space occurs for talc on Paths 1 and 2 (Fig. 7). Monomineralic talc compositions bound talc + quartz rocks, which, for a given n_F, expand initially to more magnesian compositions with subduction depth, reach a maximum, and then diminish. On Path 1, this boundary never intersects the invariant assemblage enstatite + talc + quartz, which means that for all bulk compositions, a talc + quartz assemblage cannot transform directly to enstatite + quartz; enstatite + talc assemblages will always intervene. This interesting behavior occurs because flow is assumed to take place at constant P and T, and because of the intersection of the enstatite-talc phase boundary and the quartz-saturation limit in Figure 5A. As the intersection is approached, the compositional difference between a quartz-saturated fluid and one in equilibrium with enstatite + talc diminishes to zero; at an infinitesimal distance from the intersection, an infinite amount of fluid is required to supply sufficient SiO_2 to convert enstatite to talc.

Although not shown in Figure 7, mineral modes vary within bimineralic fields. The slopes of modal isopleths within these fields are parallel to the slopes of the bounding monomineralic zones. For example, for $V^o_{fo} = 60\%$ on Path 2, flow and reaction with 2 moles of quartz-saturated fluid would produce the following

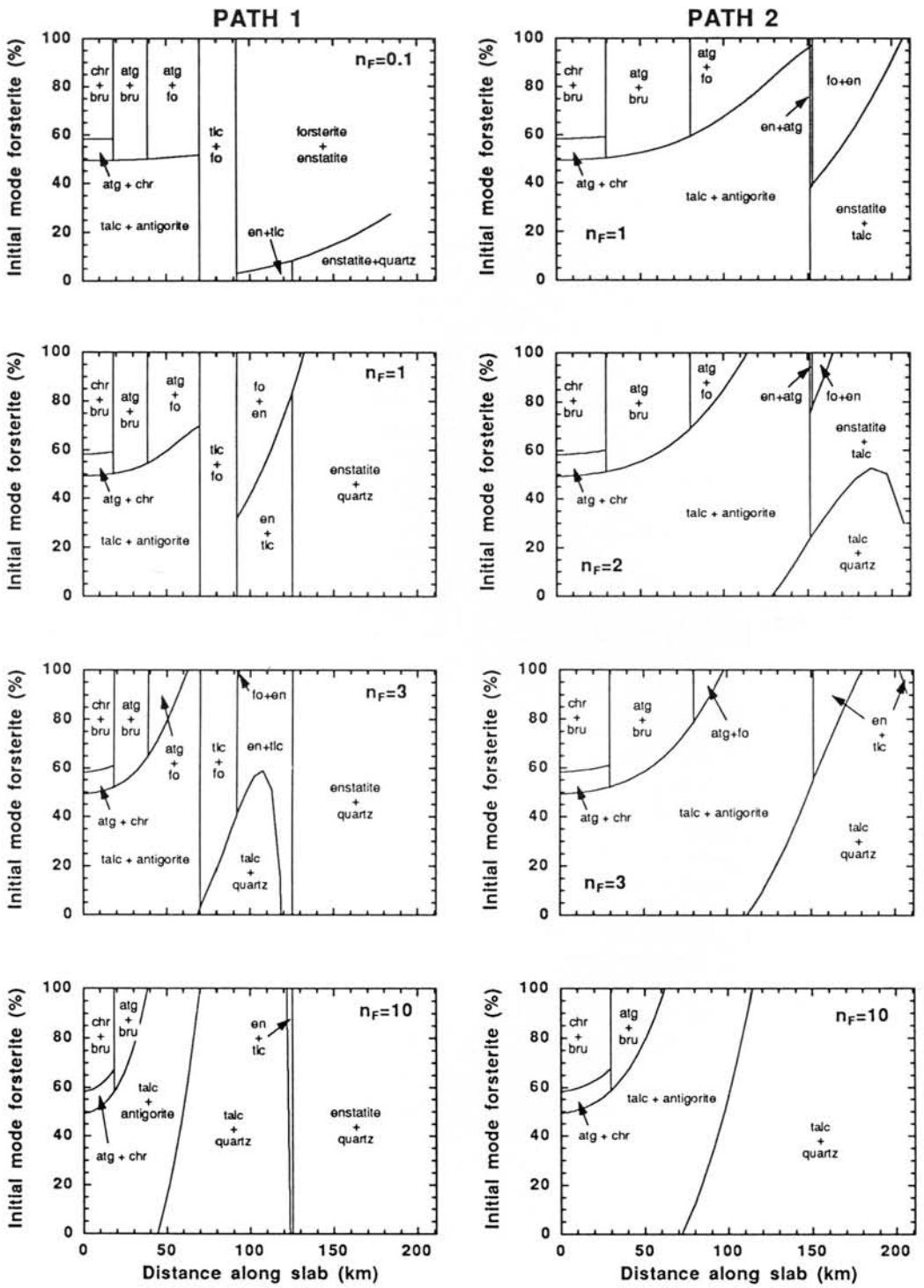

FIG. 7. Metasomatic assemblages produced by flow of different quantities of fluid as a function of starting forsterite mode and distance along the slab for each P-T path.

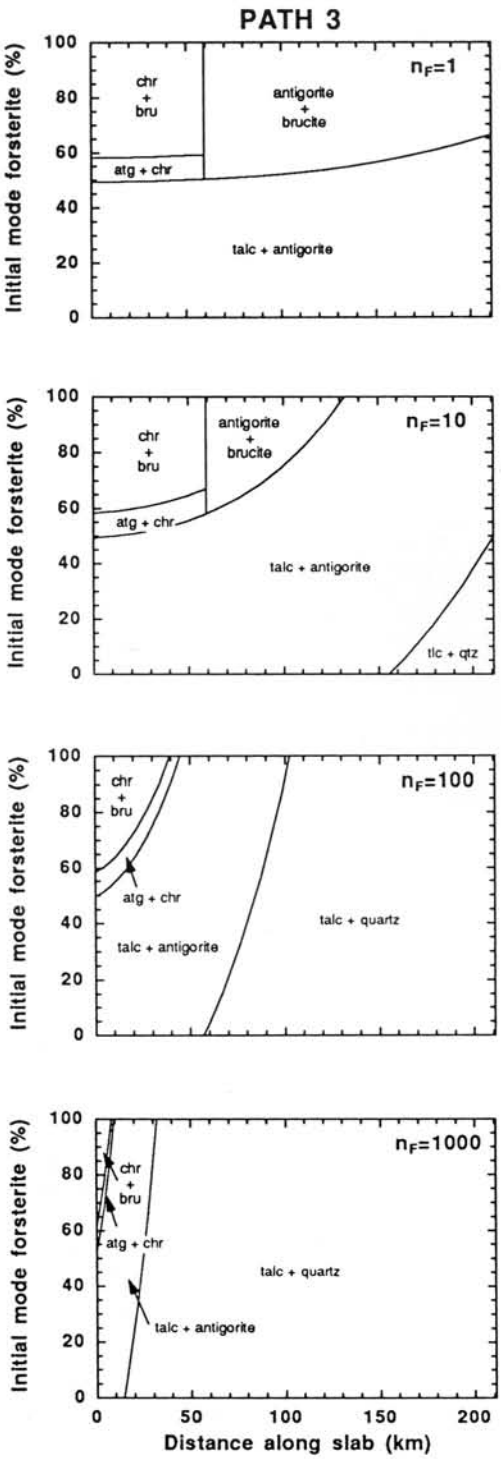

FIG. 7. (*continued*).

downdip sequence of mineral zones in which the modal abundance of the silica-rich phase increases with depth in each bimineralic field: chrysotile + brucite; chrysotile; antigorite + chrysotile; antigorite; talc + antigorite; etc. In general, because rock composition is fixed in monomineralic zones, they track changes in the spatial gradients in bulk composition with changes in the water-rock ratio. For example, values of V^o_{fo} that can be converted to pure antigorite increase with subduction depth. For a given V^o_{fo}, the depth at which it can be converted to 100% antigorite by flow at constant P and T decreases with increasing water-rock ratio.

The total amount of silica available to drive reaction also increases with increasing temperature at fixed pressure (Fig. 5). Thus, water-rock ratios required to cause a given mineralogic change decrease from Path 3 to Path 1. For example, after interaction with 10 moles of fluid, a peridotite with $V^o_{fo} = 80\%$ will consist of antigorite + brucite at 70 km along the slab on Path 3. The same conditions will produce a talc + antigorite rock on Path 2, and a talc + quartz rock on Path 1.

Discussion

For a given subduction path, Figure 7 provides chemical maps that allow specific mineral assemblages to be related to water-rock ratios if initial MSH bulk compositions are known. For collision of oceanic plates, mantle-wedge peridotites at lithospheric depths are probably similar to abyssal and alpine ultramafic rocks. Dick et al. (1984) showed that typical abyssal peridotites are spinel harzburgites with 75 ± 5% (1 S.D.) olivine, 21 ± 4% enstatite, 3.6 ± 2.0% diopside, and 0.5 ± 0.2% spinel. The average phase proportions translate to a model MSH rock of 78% forsterite and 22% forsterite. Alpine ultramafics representing oceanic mantle lithosphere are similar in modal mineralogy (Dick and Bullen, 1984). Metasomatic phase relations derived for $V^o_{fo} = 80\%$ therefore provide the closest approximation of fluid–rock interaction in natural mantle-wedge peridotites above subducting oceanic lithosphere.

For $V^o_{fo} = 80\%$, as for other bulk compositions, certain mineral assemblages are diagnostic of SiO_2 addition by fluid flow along each

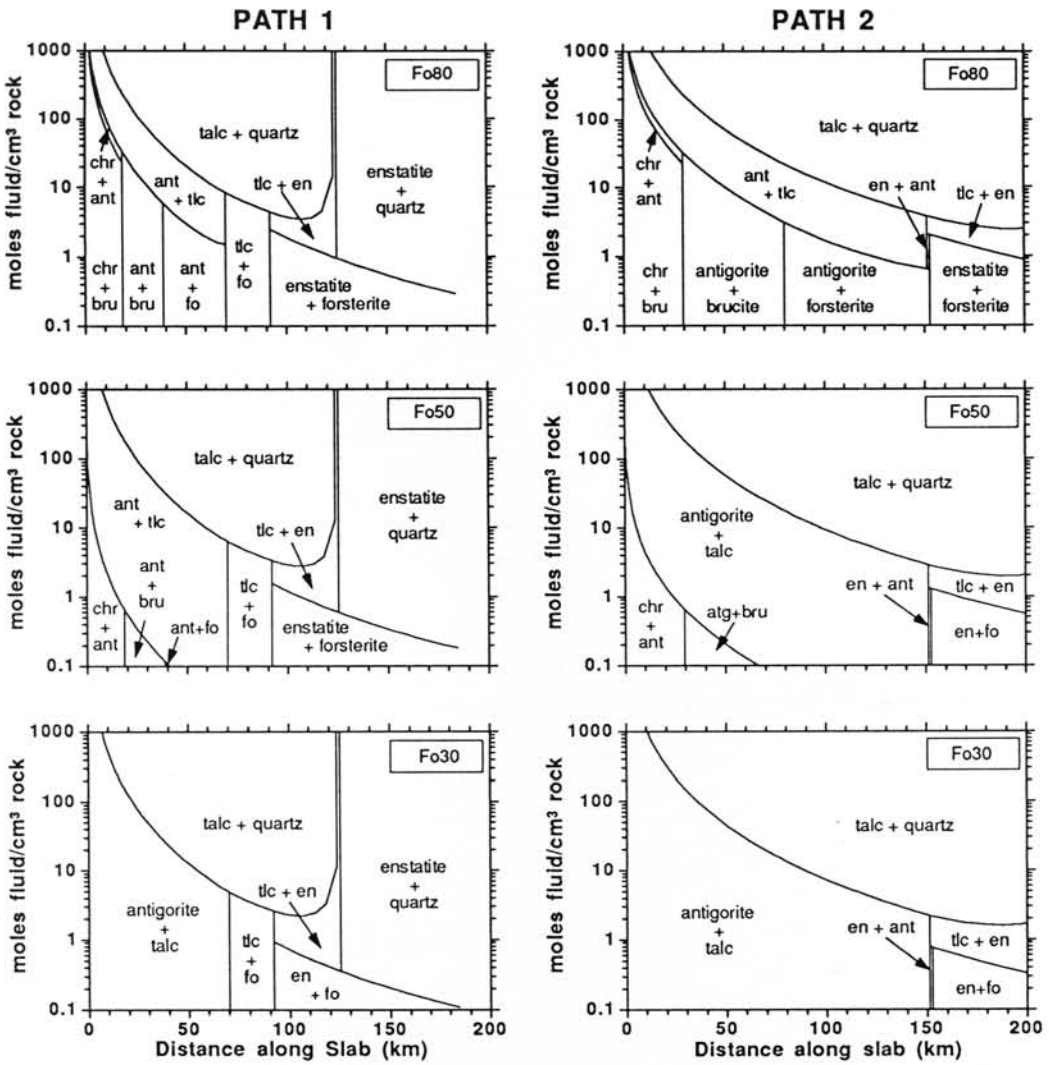

FIG. 8. Variation in water-rock ratios required to produce metasomatic mineral assemblages with distance along slab for different P-T paths and initial forsterite contents (e.g., Fo80 = 80% forsterite by volume).

path (cf. Ferry, 1994). This can be seen in Figure 8, where mineral stability fields are given in terms of position along the slab and water-rock ratio for $V^{o}_{fo} = 80\%$ (along with more siliceous bulk compositions for comparison). On Path 3, the assemblages chrysotile + antigorite, antigorite + talc, or talc + quartz require addition of silica to a peridotite with $V^{o}_{fo} = 80\%$ (Figs. 3 and 7). At $\leq$ 20 kbar, production of chrysotile + brucite requires $\geq$ 2 mol/cm^3, whereas production of talc + quartz requires more than about 15 mol/cm^3. Regardless of path, talc + quartz, talc + enstatite, and enstatite + quartz assemblages require metasomatic silica addition if the rock bulk-composition originally lies between enstatite and forsterite. Similarly, independent of bulk composition, talc + quartz implies a water-rock ratio of $>$1 mol/cm^3 and talc + enstatite and enstatite + quartz indicate $>$0.1 mol/cm^3. In addition, maximum limits on the water-rock ratio can be inferred from Figure 8 if starting fluid is known to be quartz-saturated. On the other hand, Figure 8 also illustrates the importance of knowing the pressure

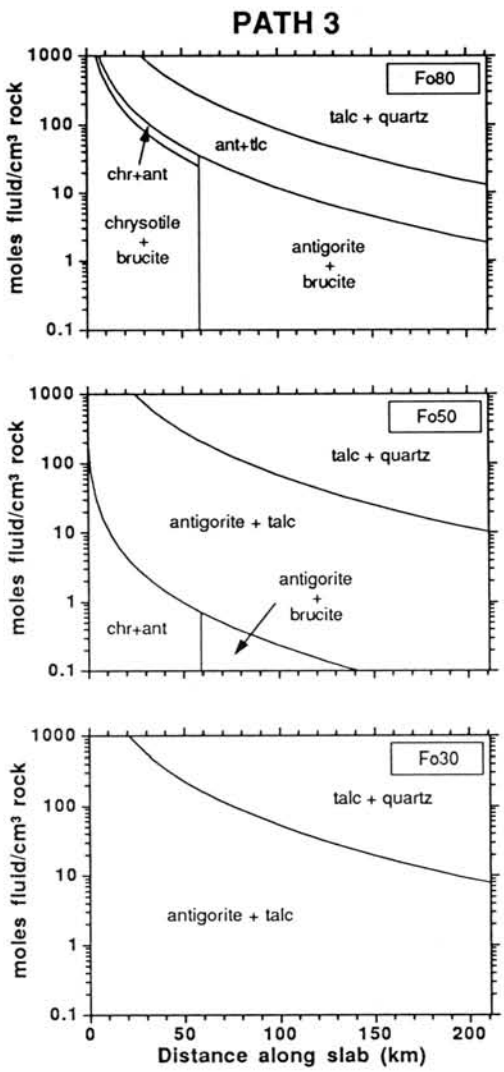

FIG. 8. (*continued*).

and temperature at which metasomatic reactions take place; for example, production of an antigorite-talc rock at $V^{o}_{fo} = 50\%$ on Path 2 may indicate anywhere from <0.1 to >100 mol/cm³, depending on location in the subduction zone.

Figure 8 also illustrates the phase-equilibrium constraints on the decrease in water-rock ratio required to drive discontinuous reactions. With the exception of the equilibrium enstatite + $SiO_{2(aq)}$ + H_2O = talc (see above), fluid volumes necessary to produce a given assemblage decrease with increasing depth, both along each path and with increasing temperature at a constant pressure. These results are not, in principle, required by the negative dP/dT of m_{SiO_2} isopleths at quartz saturation (Fig. 4); rather, they result from the negative dP/dT of all relevant m_{SiO_2} buffers presented in Table 3.

Figures 7 and 8 show that, at steady state in the deeper levels of subduction zones or along high-T subduction paths, natural mantle-wedge peridotites at the slab-mantle interface may be expected to have their bulk SiO_2 contents modified by the influx of modest quantities of fluids from the slab, similar to the changes that occur when ultramafic and siliceous rocks are juxtaposed in crustal metamorphic environments (e.g., Jahns, 1967; Evans and Trommsdorff, 1974; Frost, 1975; Evans, 1977; Sanford, 1982; Rosing, 1989). Conversely, influx of quartz-saturated fluid into natural peridotites at shallow, low-temperature portions of subduction zones is unlikely to cause obvious shifts in bulk SiO_2 content or modal mineralogy, even at high water-rock ratios. This observation is consistent with the fact that there is well-documented evidence of silica addition to peridotites in some high-temperature subduction complexes—e.g., Santa Catalina Island, California (Bebout and Barton, 1989, 1993; Bebout, 1991)—whereas extensively hydrated ultramafic rocks from low-temperature complexes display little silicification—e.g., New Idria, California (Coleman, 1961) and forearc serpentinite seamounts, Marianas (Fryer et al., 1985, 1990).

These observations, based on steady-state P-T paths, also can be extended to time-dependent changes in subduction zones. Perhaps the most important temporal change is that temperature declines as subduction zones evolve (e.g., Peacock, 1993a). This suggests that the potential for silica metasomatism is greatest at a given point in any subduction zone early in its history, which in turn implies that high-temperature silica metasomatism of ultramafic rocks in exhumed subduction complexes might contain a record of processes associated with the initial stages of subduction. Other factors favoring decreasing temperature with time—such as increasing subduction rate, greater age of subducted lithosphere, or decreasing shear stress—also will decrease the potential for silica meta-

somatism near the slab-mantle interface. Conversely, the opposite changes in these conditions will favor increasing temperature with time, and therefore will enhance the potential for silica metasomatism of the mantle wedge.

Conclusions

1. Concentrations of silica dissolved in H_2O generally are low throughout the range of subduction conditions considered ($P < 20$ kbar; $T < 1000°$ C).

2. Mineral buffers require that $SiO_{2(aq)}$ concentration in metaperidotite pore fluids increases with depth in subduction zones, regardless of P-T path or relative modal abundance of forsterite and enstatite in the starting model mantle-wedge.

3. At any given depth, $SiO_{2(aq)}$ concentration in metaperidotite pore fluids increases with temperature.

4. Water-rock ratios required to generate metasomatic mineral assemblages that differ from the hydrous equivalents of model mantle-wedge peridotites decrease with increasing pressure and temperature. At shallow levels of subduction zones, mineral assemblages diagnostic of silica metasomatism indicate water-rock ratios of > 100 moles fluid/cm^3 rock, whereas at depth, flow of several moles fluid/cm^3 rock is sufficient to produce assemblages diagnostic of silica metasomatism.

5. Decreasing temperature with time in most subduction zones suggests that the potential for silica metasomatism is greatest in the initial stages of motion along the slab-mantle interface. Subducted ultramafic rocks showing evidence of high-temperature silica metasomatism may therefore contain a record of early subduction processes. In general, temporal changes in subduction parameters favoring declining temperatures will diminish the potential for silica metasomatism, whereas those leading to higher temperatures will increase the likely extents and magnitudes of silica transfer with time.

Acknowledgments

Research from which this paper was derived was supported by NSF EAR-9405999. I thank M. Grove and H. Lin for comments on an initial draft of the manuscript.

REFERENCES

Akimoto, S., and Akaogi, M., 1980, The system Mg_2SiO_4-MgO-H_2O at high pressures and temperatures—possible hydrous magnesian silicates in the mantle transition zone: Phys. Earth Planet. Inter., v. 23, p. 268–275.

Arculus, R. J., and Powell, R., 1986, Source component mixing in the regions of arc magma generation: Jour. Geophys. Res., v. 91, p. 5913–5926.

Ayers, J. C., and Watson, E. B., 1993, Rutile solubility and mobility in supercritical aqueous fluids: Contrib. Mineral. Petrol., v. 114, p. 321–330.

Bauer, J. F., and Sclar, C. B., 1979, Crystal chemistry and stability of a high-pressure hydrous 10Å layer silicate in the system MgO-SiO_2-H_2O, *in* Timmerhaus, K. D., and Barber, M. S., eds., High-pressure science and technology (Proc. Sixth AIRAPT Conference), v. 2: New York, Plenum, p. 144–152.

———, 1981, The "10Å phase" in the system MgO-SiO_2-H_2O: Amer. Mineral., v. 66, p. 576–585.

Bebout, G. E., 1991, Geometry and mechanisms of fluid flow at 15 to 45 kilometer depths in an Early Cretaceous accretionary complex: Geophys. Res. Lett., v. 18, p. 923–926.

Bebout, G. E., and Barton, M. D., 1989, Fluid flow and metasomatism in a subduction zone hydrothermal system: Catalina Schist terrane, California: Geology, v. 17, p. 976–980.

———, 1993, Metasomatism during subduction: Products and possible paths in the Catalina Schist, California: Chem. Geol., v. 108, p. 61–92.

Berman, R. G., 1988, Internally-consistent thermodynamic data for minerals in the system Na_2O-K_2O-CaO-MgO-FeO-Fe_2O_3-Al_2O_3-SiO_2-TiO_2-H_2O-CO_2: Jour. Petrol., v. 29, p. 445–522.

Berman, R. G., Engi, M., Greenwood, H. J., and Brown, T. H., 1986, Derivation of internally-consistent thermodynamic data by the technique of mathematical programming: A review with application to the system MgO-SiO_2-H_2O: Jour. Petrol., v. 27, p. 1331–1364.

Berman, R. G., Engi, M., Greenwood, H. J., Brown, T. H., and Perkins, E. H., 1987, GEO-CALC: Software for calculation and display of pressure-temperature-composition phase diagrams: Amer. Mineral., v. 72, p. 861–862.

Bose, K., and Ganguly, J., 1995, Experimental and theoretical studies of the stabilities of talc, antigorite, and phase A at high pressures with applications to subduction processes: Earth Planet. Sci. Lett., v. 136, p. 109–121.

Brenan, J. M., Shaw, H. F., Ryerson, F. J., and Phinney, D. L., 1995, Mineral-aqueous fluid partitioning of trace elements at 900° C and 2.0 GPa: Constraints on the trace element chemistry of mantle and deep crustal fluids: Geochim. et Cosmochim. Acta, v. 59, p. 3331–3350.

Chernosky, J. V., Berman, R. G., and Bryndzia, L. T., 1988, Stability, phase relations, and thermodynamic properties of chlorite and serpentine group minerals, *in* Bailey, S. W., ed., Hydrous phyllosilicates (exclusive of micas): Washington, DC, Mineralogical Society of America, Reviews in Mineralogy, v. 19, p. 293–346.

Coleman, R. G., 1961, Jadeite deposits of the Clear Creek area, New Idria district, San Benito County, California: Jour. Petrol., v. 2, p. 209–247.

Davies, J. H., and Stevenson, D. J., 1992, Physical model of source region of subduction zone volcanics: Jour. Geophys. Res., v. 97, p. 2037–2070.

Delany, J. M., and Helgeson, H. C., 1978, Calculation of the thermodynamic consequences of dehydration in subducting oceanic crust to 10 kbar and >800° C: Amer. Jour. Sci., v. 278, p. 638–686.

Dick, H. J. B., and Bullen, T., 1984, Chromian spinel as a petrogenetic indicator in abyssal and alpine-type peridotites and spatially associated lavas: Contrib. Mineral. Petrol., v. 86, p. 54–76.

Dick, H. J. B., Fisher, R. L., and Bryan, W. B., 1984, Mineralogic variability of the uppermost mantle along mid-ocean ridges: Earth Planet. Sci. Lett., v. 69, p. 88–106.

Ellis, D. E., and Wyllie, P. J., 1979, Hydration and melting reactions in the system MgO-SiO_2-H_2O at pressures up to 100 kbar: Amer. Mineral., v. 64, p. 41–48.

Ernst, W. G., 1990, Thermobarometric and fluid expulsion history of subduction zones: Jour. Geophys. Res., v. 95, p. 9047–9053.

Eugster, H. P., and Baumgartner, L. P., 1987, Mineral solubilities and speciation in supercritical metamorphic fluids, *in* Carmichael, I. S. E., and Eugster, H. P., eds., Thermodynamic modeling of geologic materials: Minerals, fluids and melts: Washington, DC, Mineral. Soc. Amer., Reviews in Mineralogy, v. 17, p. 367–403.

Evans, B. W., 1977, Metamorphism of alpine peridotite and serpentinite: Ann. Rev. Earth Planet. Sci., v. 5, p. 397–447.

Evans, B. W., and Guggenheim, S., 1988, Talc, pyrophyllite, and related minerals, *in* Bailey, S. W., ed., Hydrous phyllosilicates (exclusive of micas): Washington, DC: Mineral. Soc. Amer., v. 19, p. 225–294.

Evans, B. W., and Trommsdorff, V., 1974, Stability of enstatite + talc, and CO_2-metasomatism of metaperidotite, Val d'Efra, Lepontine Alps: Amer. Jour. Sci., v. 274.

Ferry, J. M., 1986, Reaction progress: A monitor of fluid-rock interaction during metamorphic and hydrothermal events, in Walther, J. V., and Wood, B. J., Fluid-rock interactions during metamorphism: Berlin, Springer Verlag, p. 60–88.

———, 1994, Role of fluid flow in the contact metamorphism of siliceous dolomitic limestones: Amer. Mineral., v. 79, p. 719–736.

Frost, B. R., 1975, Contact metamorphism of serpentinite, chlorite blackwall and rodingite at Paddy-Go-Easy Pass, central Cascades, Washington: Jour. Petrol., v. 16, p. 272–313.

Früh-Green, G. L., 1994, Interdependence of deformation, fluid infiltration and reaction progress recorded in eclogitic metagranitoids (Sesia Zone, Western Alps): Jour. Metamorphic Geol., v. 12, p. 327–343.

Fryer, P., Ambos, E. L., and Hussong, D. M., 1985, Origin and emplacement of Mariana forearc seamounts: Geology, v. 13, p. 774–777.

Fryer, P., Pearce, J. A., Stokking, L. B., et al., 1990, Proc. ODP, Init. Repts., v. 125: College Station, TX, Ocean Drilling Program, 1092 p.

Gill, J. B., 1981, Orogenic andesites and plate tectonics: Berlin, Springer Verlag, 385 p.

Green, D. H., 1973, Experimental melting studies on a model upper mantle composition at high pressure under water-saturated and water-undersaturated conditions: Earth Planet. Sci. Lett., v. 19, p. 37–53.

Haar, L., Gallagher, J. S., and Kell, G. S., 1984, NBS/NRC steam tables: New York, Hemisphere.

Harlow, G. E., 1995, Jadeitites, albitites and related rocks from the Motagua fault zone, Guatemala: Jour. Metamorphic Geol., v. 12, p. 49–68.

Haselton, H. T., Jr., Chou, I.-M., Shen, A. H., and Bassett, W. A., 1995, Techniques for determining pressure in the hydrothermal diamond-anvil cell: Behavior and identification of ice polymorphs (I, III, V, VI): Amer. Mineral., v. 80, p. 1302–1306.

Hawkesworth, C. J., Gallagher, K., Hergt, J. M., and McDermott, F., 1993, Trace element fractionation processes in the generation of island arc basalts: Phil. Trans. Roy. Soc. London, Ser. A., v. 342, p. 171–191.

Hay, W. W., Sloan, J. L., II, and Wold, C. N., 1988, Mass/age distribution and composition of sediments on the ocean floor and the rate of sediment subduction: Jour. Geophys. Res., v. 93, p. 14,933–14,940.

Heinrich, C. A., 1982, Kyanite-eclogite to amphibolite facies evolution of hydrous mafic and pelitic rocks, Adula Nappe, Central Alps: Contrib. Mineral. Petrol., v. 81, p. 30–38.

Helgeson, H. C., 1967, Solution chemistry and metamorphism, *in* Abelson, P. H., Researches in geo-

chemistry, v. 2: New York, John Wiley and Sons, p. 362–404.

———, 1970, Description and interpretation of phase relations in geochemical processes involving aqueous solutions: Amer. Jour. Sci., v. 268, p. 415–438.

Helgeson, H. C., Delany, J. M., Nesbitt, H. W., and Bird, D. K., 1978, Summary and critique of the thermodynamic properties of rock-forming minerals: Amer. Jour. Sci., v. 278-A, p. 1–229.

Hemley, J. J., Montoya, J. W., Christ, C. L., and Hostetler, P. B., 1977a, Mineral equilibria in the MgO-SiO_2-H_2O system: I. Talc-chrysotile-forsterite-brucite stability relations: Amer. Jour. Sci., v. 277, p. 322–351.

Hemley, J. J., Montoya, J. W., Shaw, D. R., and Luce, R. W., 1977b, Mineral equilibria in the MgO-SiO_2-H_2O system: II. Talc-antigorite-forsterite-anthophyllite-enstatite stability relations and some geologic implications in the system: Amer. Jour. Sci., v. 277, p. 353–383.

Hostetler, P. B., and Christ, C. L., 1968, Studies in the system MgO-SiO_2-CO_2-H_2O (I): The activity product constant of chrysotile: Geochim. et Cosmochim. Acta, v. 32, p. 485–497.

Ito, E., and Weidner, D. J., 1986, Crystal growth of $MgSiO_3$ perovskite: Geophys. Res. Lett., v. 13, p. 464–466.

Jahns, R. J., 1967, Serpentinites of the Roxbury district, Vermont, *in* Wyllie, P. J., ed., Ultramafic and related rocks: New York, Wiley, p. 137–159.

Johnson, M. C., and Walker, D., 1993, Brucite [$Mg(OH)_2$] dehydration and the molar volume of H_2O to 15 GPa: Amer. Mineral., v. 78, p. 271–284.

Jones, B. F., 1986, Clay mineral diagenesis in lacustrine sediments: U.S. Geol. Surv. Bull. 1578, p. 291–300.

Jones, B. F., and Gallan, E., 1988, Sepiolite and palygorskite, *in* Bailey, S. W., ed., Hydrous phyllosilicates: Washington, DC, Mineral. Soc. Amer., Reviews in Mineralogy, v. 19, p. 631–674.

Kanzaki, M., 1991, Stability of hydrous magnesian silicates in the mantle transition zone: Phys. Earth Planet. Inter., v. 66, p. 307–312.

Khorzhinskii, D. S., 1964, An outline of metasomatic processes: Int. Geol. Rev., v. 6, p. 1713–1734.

———, 1965, The theory of systems with perfectly mobile components and processes of mineral formation: Amer. Jour. Sci., v. 263, p. 193–205.

Kitahara, S., Takenouchi, S., and Kennedy, G. C., 1966, Phase relations in the system MgO-SiO_2-H_2O at high temperatures and pressures. Amer. Jour. Sci., v. 264, p. 223–233.

Kobayashi, S., Miyake, H., and Shoji, T., 1987, A jadeite rock from Oosa-cho, Japan: Mineral. Jour., v. 13, p. 31–37.

Kushiro, I., 1970, Stability of amphibole and phlogopite in the upper mantle: Carnegie Inst. Washington Year Book, v. 68, p. 245–247.

Kushiro, I., Syono, Y., and Akimoto, S., 1968a, Melting of a peridotite nodule at high pressures and high water pressures: Jour. Geophys. Res., v. 73, p. 6023–6029.

Kushiro, I., Yoder, H. S., Jr., and Nishikawa, M., 1968b, Effect of water on the melting of enstatite: Geol. Soc. Amer. Bull., v. 79, p. 1686–1692.

Kyte, F. T., Leinen, M., Heath, G. R., and Zhou, L., 1993, Cenozoic sedimentation history of the central North Pacific: Inferences from the elemental geochemistry of core LL44-GPC3. Geochim. et Cosmochim. Acta, v. 57, p. 1719–1740.

Liu, L., 1986, Phase transformations in serpentine at high pressures and temperatures and implications for subducting lithosphere: Phys. Earth Planet. Inter., v. 42, p. 255–262.

———, 1987, Effects of H_2O on the phase behavior of the forsterite-enstatite system at high pressures and temperatures and implications for the Earth: Phys. Earth Planet. Int., v. 49, p. 142–167.

Luth, R. W., 1995, Is phase A relevant to the Earth's mantle? Geochim. et Cosmochim. Acta, v. 59, p. 679–682.

Manning, C. E., 1994, The solubility of quartz in the lower crust and upper mantle: Geochim. et Cosmochim. Acta, v. 58, p. 4831–4839.

———, 1996a, Coupled reaction and flow in subduction zones: Si metasomatism in the mantle wedge, *in* Jamtveit, B., and Yardley, B. W. D., eds., Fluid flow and transport in rocks: New York, Chapman and Hall, in press.

———, 1996b, Effect of sediment on aqueous silica transport in subduction zones, *in* Bebout, G. E., Scholl, D., Kirby, S., and Platt, J. P., eds., Dynamics of subduction: Washington, DC, American Geophysicial Union Monograph, in press.

Manning, C. E., and Boettcher, S. L., 1994, Rapid-quench hydrothermal experiments at mantle pressures and temperatures: Amer. Mineral., v. 79, p. 1153–1158.

Millhollen, G. L., Irving, A. J., and Wyllie, P. J., 1974, Melting interval of peridotite with 5.7 per cent water to 50 kilobars: Jour. Geol., v. 82, p. 575–587.

Moore, J. C., 1975, Selective subduction: Geology, v. 3, p. 530–532.

Mysen, B. O., and Boettcher, A. L., 1975, Melting of a hydrous mantle: I. Phase relations of natural peridotite at high pressures and temperatures with controlled activities of water, carbon dioxide, and hydrogen: Jour. Petrol., v. 16, p. 520–548.

Navon, O., and Stolper, E., 1987, Geochemical consequences of melt percolation: The upper mantle as a chromatic column: Jour. Geol., v. 95, p. 285–307.

Pawley, A. R., and Wood, B. J., 1995, The high-pressure stability of talc and 10Å phase: potential storage sites for H_2O in subduction zones: Amer. Mineral., v. 80, p. 998–1003.

Pawley, A. R., Redfern, S. A. T., and Wood, B. J., 1995, Thermal expansivities and compressibilities of hydrous phases in the system MgO-SiO_2-H_2O: Talc, phase A and 10 Å phase: Contrib. Mineral. Petrol., v. 122, p. 301–307.

Peacock, S. M., 1987, Serpentinization and infiltration metasomatism in the Trinity peridotite, Klamath province, northern California: Implications for subduction zones: Contrib. Mineral. Petrol., v. 95, p. 55–70.

———, 1990, Fluid processes in subduction zones: Science, v. 248, p. 329–337.

———, 1993a, The importance of blueschist → eclogite dehydration reactions in subducting oceanic crust: Geol. Soc. Amer. Bull., v. 105, p. 684–694.

———, 1993b, Large-scale hydration of the lithosphere above subducting slabs: Chem. Geol., v. 108, p. 49–59.

Peacock, S. M., Rushmer, T., and Thompson, A. B., 1994, Partial melting of subducting oceanic crust: Earth Planet. Sci. Lett., v. 121, p. 227–244.

Pearce, J. A., and Peate, D. W., 1995, Tectonic implications of the composition of volcanic arc magmas: Ann. Rev. Earth and Planet. Sci., v. 23, p. 251–285.

Perfit, M. R., Gust, D. A., Bence, A. E., Arculus, R. J., and Taylor, S. R., 1980, Chemical characteristics of island-arc basalts: Implications for mantle sources: Chem. Geol., v. 30, p. 227–256.

Plank, T., 1993, Mantle melting and crustal recycling in subduction zones: Unpubl. Ph.D. thesis, Columbia University, New York, 444 p.

Plank, T., and Langmuir, C. H., 1993, Tracing trace elements from sediment input to volcanic output at subduction zones: Nature, v. 362, p. 739–743.

Ringwood, A. E., and Major, A., 1967, High-pressure reconnaissance investigations in the system Mg_2SiO_4-MgO-H_2O: Earth Planet. Sci. Lett., v. 2, p. 130–133.

Rosing, M. T., 1989, Metasomatic alteration of ultramafic rocks, *in* Bridgwater, D., ed., Fluid movements—element transport and the composition of the deep crust: Amsterdam, Kluwer, p. 187–202.

Sanford, R. F., 1982, Growth of ultramafic reaction zones in greenschist and amphibolite facies metamorphism: Amer. Jour. Sci., v. 282, p. 543–616.

Scambelluri, M., Müntener, O., Hermann, J., Piccardo, G. B., and Trommsdorff, V., 1995, Subduction of water into the mantle: History of an alpine peridotite: Geology, v. 23, p. 459–462.

Sclar, C. B., and Carrison, L. C., 1966, High-pressure reactions and shear strength of serpentinized dunite: Science, v. 153, p. 1285–1286.

Sorenson, S. S., 1988, Petrology of amphibolite-facies mafic and ultramafic rocks from the Catalina Schist, southern California: Metasomatism and migmatization in a subduction zone metamorphic setting: Jour. Metamorphic Geol., v. 6, p. 405–435.

Stoessell, R. K., 1988, 25° C and 1 atm dissolution experiments of sepiolite and kerolite: Geochim. et Cosmochim. Acta, v. 52, p. 365–374.

Thompson, A. B., 1992, Water in the Earth's mantle: Nature, v. 358, p. 295–302.

Thompson, J. B., Jr., 1959, Local equilibrium in metasomatic processes, *in* Ableson, P. H., Researches in geochemistry, v. 1: New York, John Wiley and Sons, p. 427–457.

Ulmer, P. C., and Trommsdorff, V., 1995, Serpentine stability to mantle depths and subduction-related magmatism: Science, v. 268, p. 858–861.

Walther, J. V., and Helgeson, H. C., 1977, Calculation of the thermodynamic properties of aqueous silica and the solubility of quartz and its polymorphs at high pressures and temperatures: Amer. Jour. Sci., v. 277, p. 1315–1351.

Walther, J. V., and Orville, P. M., 1983, The extraction-quench technique for determination of the thermodynamic properties of solute complexes: Application to quartz solubility in fluid mixtures: Amer. Mineral., v. 68, p. 731–741.

Wicks, F. J., and O'Hanley, D. S., 1988, Serpentine minerals: Structures and petrology, *in* Bailey, S. W., ed., Hydrous phyllosilicates (exclusive of micas): Washington, DC, Mineral. Soc. Amer., Reviews in Mineralogy, v. 19, p. 91–167.

Yamamoto, K., and Akimoto, S.-I., 1974, High temperature and high pressure investigations in the system MgO-SiO_2-H_2O: Jour. Solid State Chem., v. 9, p. 187–195.

———, 1977, The system MgO-SiO_2-H_2O at high pressures and temperatures—stability field for hydroxyl-chondrodite, hydroxyl-clinohumite and 10 Å phase: Amer. Jour. Sci., v. 277, p. 288–312.